THE JOURNAL OF PHYSICAL CHEMISTRY A

pubs.acs.org/JPCA Article

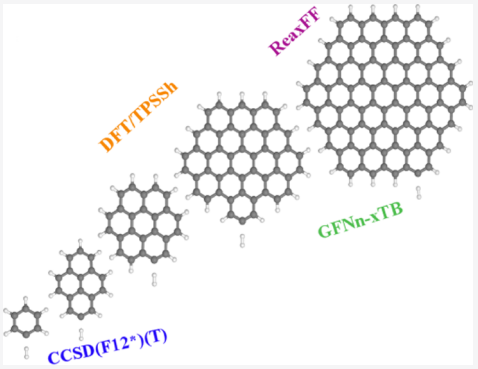
Can Small Polyaromatics Describe Their Larger Counterparts for Local Reactions? A Computational Study on the H-Abstraction Reaction by an H-Atom from Polyaromatics

Özlem Yönder,* Gunnar Schmitz,* Christof Hättig, Rochus Schmid, Paulo Debiagi, Christian Hasse, Andrea Locaspi, and Tiziano Faravelli

Cite This: J. Phys. Chem. A 2020, 124, 9626–9637 Read Online

ACCESS | Metrics & More | Article Recommendations | Supporting Information

ABSTRACT: Hydrogen abstraction is one of the crucial initial key steps in the combustion of polycyclic aromatic hydrocarbons. For an accurate theoretical prediction of heterogeneous combustion processes, larger systems need to be treated as compared to pure gas phase reactions. We address here the question on how transferable activation and reaction energies computed for small molecular models are to larger polyaromatics. The approximate transferability of energy contributions is a key assumption for multiscale modeling approaches. To identify efficient levels of accuracy, we start with accurate coupled-cluster and density functional theory (DFT) calculations for different sizes of polyaromatics. More approximate methods as the reactive force-field ReaxFF and the extended semi-empirical tight binding (xTB) methods are then benchmarked against these data sets in terms of reaction energies and equilibrium geometries. Furthermore, we analyze the role of bond-breaking and relaxation energies, vibrational contributions, and post-Hartree-Fock correlation corrections on the reaction, and for the activation energies, we analyze the validity of the Bell-Evans-Polanyi and Hammond principles. First, we find good transferability for this process and that the predictivity of small models at high theoretical levels is way superior than any approximate method can deliver. Second, ReaxFF can serve as a qualitative exploration method, whereas GFN2-xTB in combination with GFN1-xTB appears as a favorable tool to bridge between DFT and ReaxFF so that we propose a multimethod scheme with employing ReaxFF, GFN1/GFN2-xTB, DFT, and coupled cluster to cope effectively with such a complex reactive system.



INTRODUCTION

An accurate modeling of heterogeneous reactions of polyaromatic hydrocarbons with gas phase radicals is important for modeling and understanding combustion chemistry as well as soot formation. In particular, biochars are a diverse class of compounds due to the variations in the feedstock and due to the varying charring intensity applied in the production, which both affect its composition and structure.[1−4] Therefore, the effects of the structure and size of the aromatic compounds on the elementary reaction steps of biochar combustion is an important aspect for modeling its combustion.

A lot is known about reactions for small molecules,[5] but when it comes to the combustion of solid fuels such as biochar, accurate calculations on the full heterogeneous reaction systems or even on large model compounds are no longer possible. Their description is a complex multiscale problem. It requires on the small scale accurate first-principle quantum chemistry methods to obtain accurate thermodynamic data for elementary reaction steps. On the (super-)nanometer scale, force-field or coarse-grained force-field methods[6] have to be applied to generate realistic structure models, and in between, efficient tools are needed to select, out of the myriads of, in principle, thinkable reaction steps, those that could be relevant. In the context of heterogeneous combustion, where covalent bond breaking needs to be described, reactive force fields, for example, ReaxFF,[7] developed by van Duin et al., are often used to deal with the mere size of the system, however, oftentimes relying solely only on this approximate method.[8−10]

The limitation of accurate quantum chemistry methods to small systems raises the question whether, or to which extent, an analogy between gas phase reactions and heterogeneous reactions exists.[11] Detailed or semi-detailed mechanisms as commonly employed in computational fluid dynamics simulations involving heterogeneous gas/solid reactions adopt rate constants derived from analogous gas-phase reactions[12] or accounting for proper corrections proposed about 30 years ago

Received: August 4, 2020
Revised: September 17, 2020
Published: November 4, 2020



Downloaded via BOCHUM LIBRARIES on November 30, 2020 at 19:40:00 (UTC).
See https://pubs.acs.org/sharingguidelines for options on how to legitimately share published articles.

ACS Publications © 2020 American Chemical Society

https://dx.doi.org/10.1021/acs.jpca.0c07133
J. Phys. Chem. A 2020, 124, 9626–9637

by Frenklach and Wang.[13] These assumptions require specific validations. Some preliminary results show that the activation energies of H-abstractions on graphene edges by different radicals can be related to those of the analogous reactions in the gas phase.[11] For a multiscale modeling of biochar combustion, important questions are thus how transferable are results for reaction and activation enthalpies on small polycyclic aromatic hydrocarbons (PAHs) to larger systems and to which extent can results that are obtained with cost-efficient force-field and semi-empirical methods be combined with accurate electronic structure calculations. With this study, we aim to contribute to this question with the specific example of the hydrogen abstraction reactions of PAHs. This reaction has the importance as an initiation step for combustion and especially for soot formation through the hydrogen abstraction C_2H_2 addition (HACA) mechanism.[14]

In a recent study on the H-abstraction reactions on armchair and zigzag edges of graphene, it has been shown that the interactions between the layers do not affect the transition state and reaction barriers.[11] Therefore, we do not describe here the effect of the different numbers of layers on this reaction. In the current study, we use a test set of PAHs ranging from benzene to $C_{96}H_{24}$ that, apart from varying in size, exhibit a variety of reaction sites that represent different situations such as zigzag, armchair, or free edges.[15] As quantum chemistry electronic structure methods, we employ density functional theory (DFT) with a modern meta-GGA hybrid functional. For the smaller PAHs, these are combined with single point coupled-cluster (CC) calculations. Apart from the costly CC calculations which are only possible for small- and medium-sized molecules, a bottleneck for larger PAHs are the searches for the transitions states. Here, the questions are (1) how transferable are differences between DFT and CC energies from the small to the larger PAHS and (2) how well the activation energies correlate with the reactions energies (Bell−Evans−Polanyi principle),[16,17] that is, how accurate can activation energies be estimated based on it?

Individual local reaction can be targeted directly with static DFT and coupled-cluster calculations. A route to complex sequences of reactions, as they occur during the combustion of char, which is tractable for first-principles calculations is to preselect the most important elementary steps based on reactive molecular dynamics. This requires cost-efficient semi-empirical electronic structures or reactive force-field methods. To investigate their performance in the context of combustion, we do a similar assessment for the extended semi-empirical tight-binding methods xTB (GFN0-xTB, GFN1-xTB, and GFN2-xTB)[18,19] of Grimme and co-workers as well as for the reactive force-field ReaxFF.[7] Again, the aim is to compare these more approximate methods with the more accurate DFT and CC results. We compare reaction energies and geometrical similarity of stationary points on the potential energy surface (PES) such as minima and transition states. For modeling the combustion of solid fuels, it is vital to have cost-efficient methods which qualitatively and semi-quantitatively reproduce the correct PES. In this case, those methods can be used, as pointed out above, for prescreening or, for less local reactions, combined in hybrid approaches, where larger parts are optimized using ReaxFF or xTB and smaller active sites are optimized using DFT. Furthermore, only these methods scale efficiently enough to be applied in large scale molecular dynamic simulations to get an understanding on the atomistic scale of the processes involved in combustion.

COMPUTATIONAL DETAILS

For the current study, we have selected a test set consisting of 13 PAHs which range in size from benzene to $C_{96}H_{24}$, as shown in Figure 1. These PAHs cover a variety of reaction sites such as

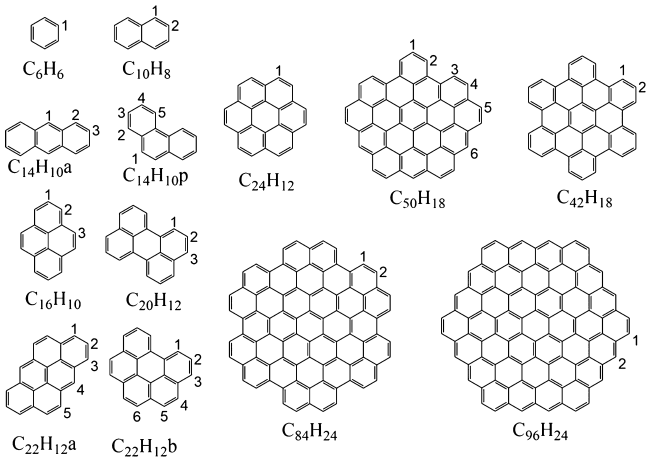


Figure 1. Selected reaction sites.

sterically unhindered sites at zig-zag, free edges (e.g., in $C_{96}H_{24}$), and sterically hindered bay region sites at armchair edges (e.g., the sites 1 in $C_{20}H_{12}$, $C_{42}H_{18}$, or $C_{84}H_{24}$). For details of the nomenclature for the sites, see Supporting Information.

All geometries have been optimized at the DFT level (vide infra). At the same level, we have also calculated the analytical second derivative of the PES with the harmonic approximation, from which the vibrational contributions are evaluated. For a few cases, we carried out explicitly correlated coupled cluster, CCSD(F12*)(T), and for a larger subset local pair-natural orbital coupled cluster, PNO-CCSD, calculations.

In this study, the performance of the DFT functional is important for the calculation of zero point vibrational energies (ZPVEs) and the partition functions, as well as for observing the general trends in the activation and reaction energies. Therefore, we have used the TPSSh functional. In a previous study, it was stated that for the H abstraction reaction with the H atom and methyl radical, the TPSSh functional has a mean absolute error of up to 38 kJ/mol as compared with G3(MP2)-RAD results; therefore, the PBE0 functional was recommended.[20] On the other hand, based on the C3/99 test set, the TPSSh functional performs as good as the most common hybrid functionals, such as PBE0 or B3LYP, for bond lengths, angles, bond dissociation energies, and the harmonic vibrational frequencies, and it outperforms them for the calculation of standard enthalpies of formation.[21]

The DFT calculations have been performed using TURBOMOLE's m5 integration grid[22] (except for reactions of $C_{84}H_{24}$ and $C_{96}H_{24}$ for which m3 grid is used), TZVP basis set,[23] and Grimme's D3 dispersion correction[24] and were performed with the dscf, grad, and aoforce programs of the TURBOMOLE package.[25] The zero-point vibrational energy (ZVPE) corrections to the electronic energies were computed at the same electronic structure level (TPSSh-D3/TZVP) within the harmonic approximation. We have used the scaling factor of 0.9874 for TPSSh/6-31+G(d,p) to fit the experimental ZPVE.[26]

All CC calculations employed the frozen core approximation for the $1s^2$ electrons on carbon. To obtain it for the smaller molecules, results close to the basis set limit, we used the

https://dx.doi.org/10.1021/acs.jpca.0c07133
J. Phys. Chem. A 2020, 124, 9626−9637

Table 1. Deviations in the C−H Bond Distance (in pm) and C−C−C Angle (in deg) for the Semi-empirical and FF Methods Compared to the TPSSh-D3/TZVP Reference Structure[a]

	PAHs				H-abstracted			
	GFN0-xTB	GFN1-xTB	GFN2-xTB	ReaxFF	GFN0-xTB	GFN1-xTB	GFN2-xTB	ReaxFF
				C−H Distance				
|MAX|	0.220	0.130	0.510	1.400	0.240	0.220	0.590	1.480
MEAN	−0.039	0.006	0.438	0.757	−0.046	0.006	0.432	0.657
RMSD	0.069	0.056	0.439	0.818	0.081	0.069	0.433	0.768
				C−C−C angle				
|MAX|	1.49	1.54	1.57	3.49	5.22	4.95	4.96	28.35
MEAN	0.04	0.07	0.06	−0.08	0.01	0.03	0.02	−0.48
RMSD	0.28	0.32	0.29	0.86	0.66	0.41	0.39	4.46

[a]It is differentiated between the native PAHs structures and the H abstracted radical structures.

explicitly correlated CCSD(F12*) approach[27] with the aug-cc-pVTZ orbital,[28] corresponding optimized complementary auxiliary,[29] and density-fitting basis[30] sets. The reference Hartree−Fock determinants are calculated using the dscf program,[31] the CC singles, doubles, and perturbative triples, CCSD(F12*)(T), and calculations for the reactions of benzene and naphthalene are performed using the ccsdf12 program.[25] For the PAHs up to $C_{24}H_{12}$, we did local pair natural orbital (PNO) based ROHF-CCSD, also known as UR-CCSD, calculations in the cc-pVTZ basis using a local development version of the pnoccsd program.[32−34] For anthracene and phenanthrene, we did in addition PNO-UHF-CCSD(F12*)(T) calculations to investigate the trend of coupled-cluster methods based on UHF reference determinants with the size of PAHs.

The ReaxFF calculations were performed using the reimplementation of ReaxFF[35] available in the LAMMPS Molecular Dynamics Simulator[36] and using the "CHO" parameterization for combustion, as published in ref 37. The xTB calculations were done with version 6.3.1 of the xTB code.[18,19,38] If not otherwise stated, we used in all calculations the standard settings in xTB. For the transition state optimization with xTB, we interfaced it to the TURBOMOLE reaction pathfinder statpt[39] and the transition state optimizer statpt.

The reaction rate constants have been calculated using transition state theory (TST). The partition functions are calculated based on a modification to the quasi rigid rotor and harmonic oscillator approximation.[40] The modification is that for the low lying modes (ω < 300 cm^{-1}), the rotational and harmonic oscillator approximations are combined for partition functions instead of the entropy. In other words, for the low lying modes, the Head-Gordon damping function ($W(\omega)$) is applied to its contribution q to the partition function as

$$q = q_{vib}^{W(\omega)} q_{rot}^{1-W(\omega)} \tag{1}$$

instead of to the entropy as in the original approach[40] given by

$$S = W(\omega)S_{vib} + [1 - W(\omega)]S_{rot} \tag{2}$$

Using the ideal gas law as the equation of state, the site-specific forward reaction rate constants without using symmetry numbers are calculated at 1 bar based on the TST according to

$$k_{forward}(T) = \kappa \frac{RT}{P} \frac{k_B T}{h} \frac{Q_{TS}}{Q_{PAH} Q_H} \exp\left(-\frac{E_{el,act}}{RT}\right) \tag{3}$$

where R is the gas constant, P the pressure, k_B the Boltzmann's constant, T the temperature, h Planck's constant, and Q_{TS}, Q_{PAH}, and Q_H are the partition functions which include translational, vibrational, and rotational contributions, respectively. The vibrational partition function is defined relative to the bottom of the PES, and $E_{el,act}$ is the electronic activation energy (without the ZPVE). κ is the transmission coefficient used to account for tunneling. It is calculated using the high temperature limit of the Eckart tunneling correction, which asymptotically approaches to Wigner tunneling correction[41]

$$\kappa = 1 - \frac{1}{24}\left(\frac{h\nu}{k_B T}\right)^2 \left(1 + \frac{RT}{E_{el,act}}\right) \tag{4}$$

In eq 4, ν is the imaginary frequency at the transition state.

RESULTS

Geometrical Accuracy of Semi-empirical Methods and Reactive Force Fields. DFT methods give (usually) accurate geometries and, with hybrid functionals, reasonable reaction and activation energies but are, although computationally much less demanding than coupled-clusters methods, still computationally costly. If one is interested in large scale atomistic simulations or molecular dynamic simulations on long time scales, there is no way around more approximate but numerically more efficient methods. Here, we want to answer the question if the extended tight binding models xTB and the reactive force-field ReaxFF can be used as a bridge from DFT to larger scales. In a first step, we compare how well equilibrium geometries on the xTB and ReaxFF level agree with the DFT results and later judge on how accurate reaction energies are reproduced.

For the first purpose, we reoptimized the PAH structures and the H-abstracted structures on this level and compared the C−H bond lengths and the C−C−C angles in the aromatic rings. The reoptimization will result in smaller deviations than an optimization from other starting guesses, but this is intended. We want to assess how much the semi-empirical methods need relaxation in the found DFT minima.

The results are given in Table 1. The trend for the bond lengths is quite interesting: GFN0-xTB and GFN1-xTB reproduce the DFT equilibrium C−H bonds quite well, and the deviations increase for GFN2-xTB. This, however, does not translate into a better agreement in reaction energies for GFN0 and GFN1 (vide infra). For GFN2-xTB, we observe a RMSD in the C-H bond length of 0.43 pm for the H-abstracted species and 0.44 pm for the PAHs. This is a very consistent error for different molecular species (radical and no radical). For ReaxFF, we see a slightly more unbalanced description. For the PAHs, a RMSD of 0.082 pm is observed, while the C-H distances for the H-abstracted species deviate by an RMSD of 0.768 pm. When looking at the C−C−C angles, we see for the xTB methods a

https://dx.doi.org/10.1021/acs.jpca.0c07133
J. Phys. Chem. A 2020, 124, 9626−9637

quite good agreement, but the deviations are typically larger for the H-abstracted species. This especially holds for ReaxFF, where a RMSD of 4.43° is observed. For the radical structure, ReaxFF favors straightened C−C−C angles, which distorts the ring structure, which is presumably due to the fact that in ReaxFF, there is no concept of a radical, and a two coordinate carbon naturally tends toward a linear geometry (sp-hybridization).

It turned out to be difficult to optimize the transition states using the xTB methods and ReaxFF. For the latter case, we observed a rather non-smooth PES with large changes of the gradients in the region of the barrier, explaining the short timesteps necessary for energy-conserving MD. We located the barrier by a nudged elastic band calculation for the benzene case but refrained from an investigation of larger PAHs. Using the xTB methods, it was more straightforward to optimize transition states, but only GFN1-xTB showed a good agreement with the TPSSh-D3/TZVP-optimized structures, and since our ultimate goal is to bridge the scale from DFT calculations to larger scales, we propose to use GFN1-xTB for geometry optimizations and GFN2-xTB for energies. The results for geometrical deviations of the GFN1-xTB-optimized transition states are listed in Table 2. Especially, for the C−H bond distance (for the abstracted H atom), the deviations are larger compared to our results for the PAHs, but we see a reasonable agreement.

Table 2. Deviations in the C−H Bond Distance (in pm) and C−C−C Angle (in deg) for GFN1-xTB Compared to the TPSSh-D3/TZVP Reference Structure for the Transition State

	C−H	C−C−C
|MAX|	42.48	4.06
MEAN	−3.69	−1.26
RMSD	7.25	1.50

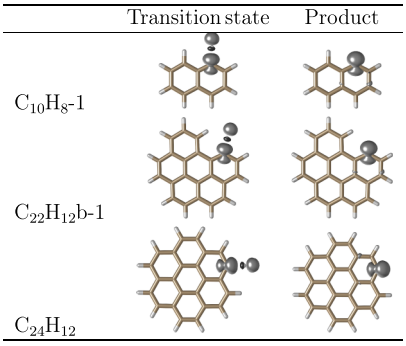
Trends from DFT. To study the abstraction of a hydrogen from PAHs, we considered the following reactions with atomic hydrogen

$$C_nH_m + H \rightarrow C_nH_{m-1} + H_2 \quad (5)$$

The reaction does not disturb the resonance in the π-system and should thus cause only local changes in the geometry and the electronic structure. As shown for some examples in Table 3, the spin density at the transition states and for the H-abstracted radicals looks very alike for any given system in this study.

Due to the local electronic character of the reaction, the electronic reaction and activation energies for this reaction are expected to be very similar and independent of the size of the polyaromatic. In accordance with this, the electronic activation energies differ only by 3.2 kJ/mol. The electronic activation energy is on average 35.6 kJ/mol, while the lowest one is 34.8 kJ/mol for $C_{22}H_{12}$a-2 and the largest one is 37.9 kJ/mol for $C_{84}H_{24}$-2. Even if the electronic activation energies are similar, the reaction energies at the sterically hindered sites ($C_{14}H_{10}$p-5, $C_{20}H_{12}$-1, $C_{22}H_{12}$b-1, $C_{42}H_{18}$-1, $C_{50}H_{18}$-2, $C_{50}H_{18}$-3, and $C_{84}H_{24}$-1) are lower than those at the sterically unhindered sites, with an average electronic reaction energy of 14.0 kJ/mol, whereas the average of those which are not sterically hindered is 21.2 kJ/mol. This can be explained by the unfavorable repulsion between the neighboring H atoms in the bay region sites, which is removed by the H-abstraction.

Table 3. Spin Densities of the Transition States and the H-Abstracted Product Radicals for Some Example Reaction Sites Calculated with DFT/TPSSh-D3/TZVP



The two determining contributions to the electronic reaction energies—for which one can expect a different sensitivity to the electronic structure method and the model compound size—are (1) the changes in the electronic structure upon removal of the H atom, that is, unrelaxed C−H bond breaking and H−H bond formation, and (2) the relaxation of the structure of the H-abstracted PAH during the geometry optimization, which is exothermic. To measure these two contributions, we calculated in addition to the reacting species also the energies of the H-removed educt structures ($E_{\text{H-removed PAH}}$) and defined the mentioned two contributions as

$$E_{C-H} = E_{\text{el,H-removed PAH}} + E_{\text{el},H_2} - E_{\text{el,PAH}} - E_{\text{el,H}} \quad (6)$$

and

$$E_{\text{relax}} = E_{\text{el,geoopt. H-abstracted PAH}} - E_{\text{el,H-removed PAH}} \quad (7)$$

which sum up to the electronic reaction energy for reaction 5

$$E_{\text{el,rxn}} = E_{C-H} + E_{\text{relax}} \quad (8)$$

Figure 2 shows the contributions to the reaction energy for different sites in a stack plot. E_{C-H} depends on the local environment of the site where the hydrogen is removed, which is strongly supported by the fact that this contribution is on average 7.0 kJ/mol less endothermic for the bay region reaction sites than those which are not sterically hindered. Additionally, it can be seen that E_{relax} does not vary much between different sites or with the size of the polyaromatics. This is also the case for the zero-point vibrational contribution to the reaction energy, which for our test set is −6.9 kJ/mol with a standard deviation of ±0.8 kJ/mol and a maximum deviation of ±2 kJ/mol. Therefore, for the H abstraction reaction, variations in the reaction energies are mainly due to unrelaxed bond breaking and formation energies, which are dependent on the local environment of the reacting site but are also independent of the size of the polyaromatic.

The reaction and activation energies of the sites without steric hindrance follow the Bell−Evans−Polanyi principle with an R^2 value of 0.9, and for the bay region sites, the correlation is less good with an R^2 value of 0.8, (Figure 3). The fact that the sterically hindered bay region sites do not fit into the BEP correlation found for the sites without steric hindrance has also been observed in previous studies.[42] Figure 4 shows that there is a correlation between the C−H distance at the transition states and the reaction energies (Hammond's postulate). Here, for the bay region sites, there is no correlation because the range of reaction energies is too small (2 kJ/mol) to observe this.

https://dx.doi.org/10.1021/acs.jpca.0c07133
J. Phys. Chem. A 2020, 124, 9626−9637

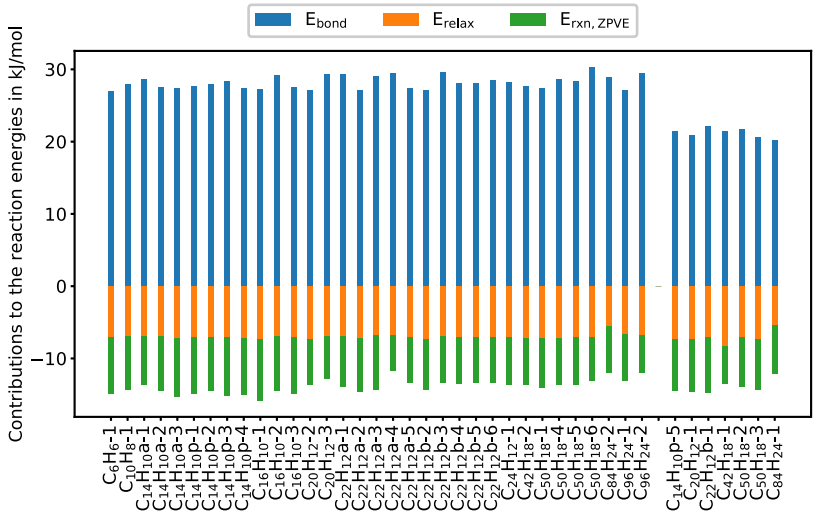


Figure 2. Stack plot of the contributions to the electronic reaction energy at the DFT/TPSSh-D3 level. The ZPV energies are stacked on top of the relaxation energies. Note that the last seven sites are the bay region sites.

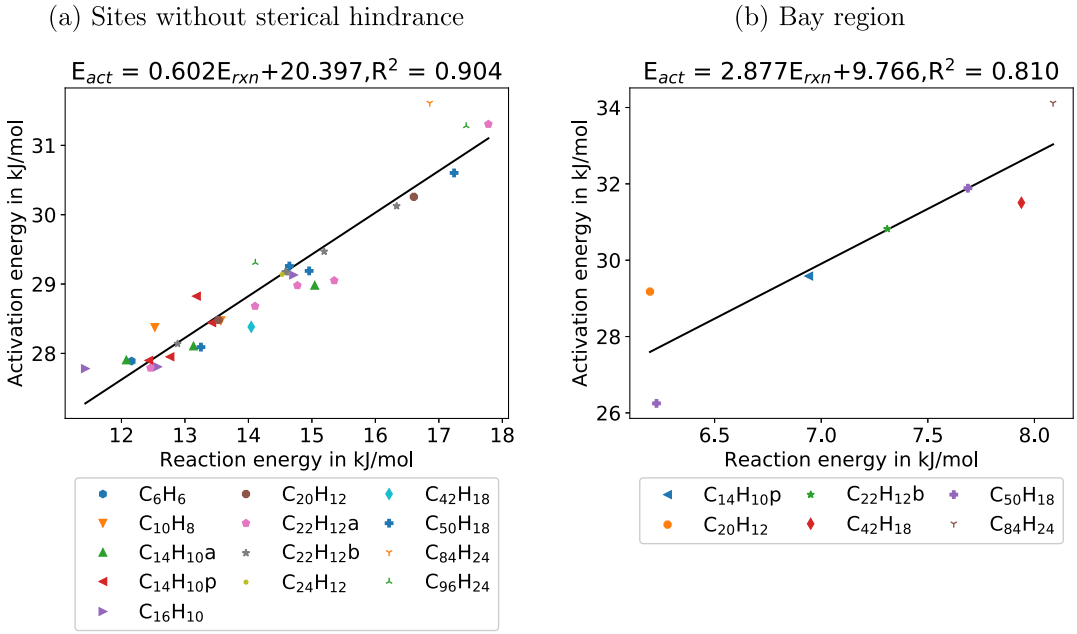


Figure 3. Relation between the reaction and activation energies (E_{rxn} and E_{act}) based on the TPSSh-D3/TZVP results.

Assessment of Semi-empirical and Reactive Force-Fields. Next we turn to a comparison of the xTB and ReaxFF reaction energies to our more accurate results, which will be presented in the subsequent sections. First, we will do a comparison to our TPSSh-D3/TZVP results and a composite scheme, based on PNO-CCSD and an extrapolation estimate for larger PAHs, which will be discussed in the sections "Coupled-Cluster Energy Corrections" and "Extrapolation to Larger PAHs". We solely concentrate on the electronic contribution to the reaction energy to allow for a better comparison. First, we will discuss the examples given in Table 4. In these cases, we see that GFN0-xTB is qualitatively not correct by a large magnitude, and GFN1-xTB starts to be at least qualitatively correct but underestimates the reaction energy nearly by a factor of 10. However, GFN2-xTB on the other hand shows a good agreement with our CC results but overestimates the reaction energy compared to the DFT results by a factor of two. Table 5 shows the average deviations of the xTB methods to the TPSSh-D3/TZVP results and the composite scheme. As for the already discussed example, GFN0-xTB is qualitatively not correct, and also, on average, GFN1-xTB is qualitatively not correct, but this is the result of a few outliers. For GFN2-xTB, the reaction energies are always qualitatively correct, but the average deviation is around 26 kJ/mol to the DFT reference and 6 kJ/mol to the composite scheme. Typically, the GFN2-xTB reactions energies are a factor of 2−2.5 larger than the DFT results and only slightly above the more accurate results given by the composite scheme. This is a positive finding since it allows us to use GFN2-xTB for prescreening of reactions and to use DFT or CC only for more accurate calculation for the reactions kept after the pre-screening. Although in our study GFN2-xTB seems to be more accurate than TPSSh-D3, we do not claim that this holds in general, and although the reaction energies are in better agreement with our most accurate reference, there were some problems with calculating activation energies on the GFN2-xTB level of theory.

https://dx.doi.org/10.1021/acs.jpca.0c07133
J. Phys. Chem. A 2020, 124, 9626−9637

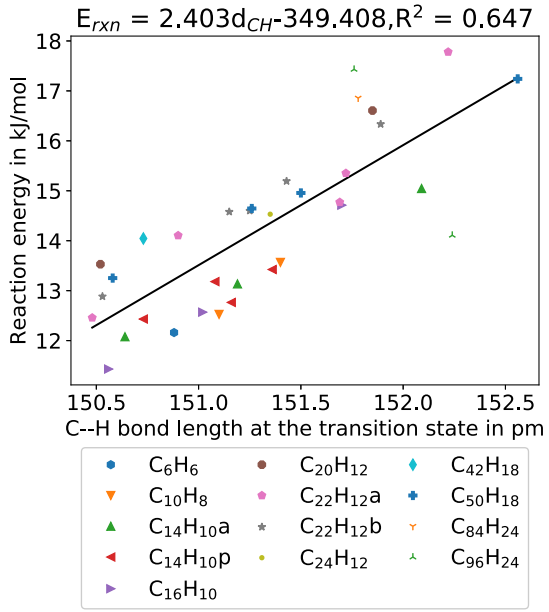


Figure 4. Reaction energies as a function of the C−H bond length of the transition state based on the TPSSh-D3/TZVP results for the sites without sterical hindrance.

In Table 4, we also give results for ReaxFF reaction energies. They are always qualitatively correct but overestimate the reaction energy on average by a factor of 4−5 with respect to the DFT reference. Compared to the composite scheme, the reaction energies improve a bit but are still 2.5−3.5 times larger than the reference values. Furthermore, we see that the reaction energy for ReaxFF is very site-dependent, which originates from ReaxFF favoring a sp^2 hybridization. Due to steric hindrance, this relaxation is not possible in all cases. The sites $C_{10}H_8$-1 and $C_{10}H_8$-2 are a good example since their reaction energies differ more than a factor of two. For $C_{10}H_8$-1, we can measure a C−C−C angle of 147.5°, while for $C_{10}H_8$-2, we observe an angle of 151.6°. Therefore, the product could in the second case relax more to its preferred state, which gives a lower reaction energy. One can conclude that ReaxFF should be used for aromatic ring-like systems in case of radicals with caution. Since the functional form for ReaxFF is not that flexible it is questionable if a different parameterization can cure this behaviour.

Besides the total electronic reaction energy, we were interested in the contribution, which stems from relaxation. This answers the question how well relative changes in a particular configuration are transferable from the semi-empirical methods to DFT. Table 6 shows the statistics over the deviations to the DFT reference. One has to note that the statistics look much better than that for the reaction energies, but still the hierarchy GFN0-xTB < GFN1-xTB < GFN2-xTB is retained. GFN1-xTB has a slightly better RMSD, but its outliers are smaller. The xTB methods seem to be accurate enough to describe the configurational changes. The relaxation in the ReaxFF optimized structures is approximately 10 times larger than that in the DFT reference, which results in large deviations with an RMSD around 75 kJ/mol, but this finding is not completely unexpected. When analyzing the deviations in the geometries, we already found that ReaxFF tends to straighten the C−C−C angle, which results in a large rearrangement and thus to a large relaxation energy.

In accordance with the overestimated reaction energies, also the reaction barrier for C_6H_6-1 is with 89 kJ/mol overestimated by a factor of about 3 for ReaxFF. In contrast to the electronic structure methods (xTB and DFT), the reactive force field also results in a non-linear arrangement of the C−H−H group at the barrier with an angle of 147°. For the assessment of the xTB reaction barriers, we used the GFN1-xTB geometries in combination with GFN1-xTB and GFN2-xTB energies to calculate the barrier heights. We compare the electronic contribution and the ZPVE contribution. A statistic for the comparison to the TPSSh-D3/TZVP results can be found in Table 7. The xTB methods underestimate the electronic contribution to the activation energy compared to the reference. GFN1-xTB predicts on average 5.9 times lower activation energies, while GFN2-xTB predicts on average 1.5 times lower barriers. For the contribution of the ZPVE, GFN1-xTB and GFN2-xTB have comparable errors but with different trends. GFN1-xTB underestimates the energies, while GFN2-xTB overestimates them. Excluding $C_{10}H_8$-1 as outlier, GFN2-xTB gives ZPEs which are on average 1.6 times larger than the TPSSh-D3/TZVP ones, while GFN1-xTB gives 0.4 times smaller ones.

Based on our gathered data, we can conclude that a combination of GFN1-xTB and GFN2-xTB is a good candidate to bridge the presented CC and DFT calculations to larger scales for the energetics GFN2-xTB is close to our CC and DFT reference, while GFN1-xTB performs better for geometry optimizations. The failure of GFN0-xTB is unfortunate since it is roughly 10 times more efficient than GFN2-xTB which would greatly improve the simulation time in MD studies, but in the case of H abstraction, GFN0-xTB overestimates the stability of molecular hydrogen. When rescaling the energy of atomic hydrogen to mimic the H_2 binding energy of CCSD(F12*), we obtain reaction energies slightly above those for GFN1-xTB. For individual reactions, such a correction term is feasible but not when used in MD simulations. GFN1-xTB and GFN2-xTB are more accurate than ReaxFF for our purposes, but since ReaxFF is still at least by a factor of 10 more efficient than GFN0-xTB, it can be a viable building block for a multiscale approach.

Table 4. Comparison of the Reaction Energies (in kJ/mol) on the Semi-empirical Level to the TPSSh-D3/TZVP, PNO-CCSD/cc-pVTZ, and ROHF-CCSD(F12*)(T)/aug-cc-pVTZ Results

	$E_{el,rxn}$						
site	GFN0-xTB	GFN1-xTB	GFN2-xTB	ReaxFF	PNO-CCSD	CCSD(F12*)(T)	TPSSh
$C_{10}H_8$-1	−189.2	4.5	49.3	107.6	47.3	43.6	20.94
$C_{10}H_8$-2	−188.0	4.9	49.7	49.0	46.8	42.7	27.60
$C_{14}H_{10}$a-1	−191.3	4.0	48.6	146.4	42.8		16.44
$C_{14}H_{10}$a-2	−189.8	4.2	48.8	105.2	41.1		15.35
$C_{14}H_{10}$a-3	−188.5	4.8	49.6	63.2	40.4		14.92
C_6H_6-1	−186.1	5.7	50.5	30.5	39.9	42.7	12.20

https://dx.doi.org/10.1021/acs.jpca.0c07133
J. Phys. Chem. A 2020, 124, 9626−9637

Table 5. Statistics of the Deviations in the Electronic Contribution of Reaction Energies (in kJ/mol) of the Semi-empirical Methods and ReaxFF Compared to Either the TPSSh-D3/TZVP Reference Values or Our Most Accurate Reaction Energies Based on the Composite Scheme, Presented in the Subsequent Sections[a]

	TPSSh-D3 reference				composite reference			
	GFN0	GFN1	GFN2	ReaxFF	GFN0	GFN1	GFN2	ReaxFF
|MAX|	220.94	27.55	30.09	154.55	239.80	45.04	9.71	117.68
MEAN	−213.36	−18.18	26.08	79.98	−228.71	−35.16	4.46	51.74
RMSD	213.38	18.50	26.33	87.03	230.73	38.73	5.88	60.07

[a]We only give the xTB parameterization GFN*n* and drop "xTB".

Table 6. Error Statistics for the Relaxation Contribution to the Reaction Energy (in kJ/mol) for the Different Semi-empirical Methods and ReaxFF Where the TPSSh-D3/TZVP Results Serve as the Reference[a]

	GFN0-xTB	GFN1-xTB	GFN2-xTB	ReaxFF
		Non-Bay Area		
|MAX|	6.56	5.56	3.87	135.78
MEAN	3.67	1.11	1.17	−74.47
RMSD	3.88	1.82	1.81	77.49
		Bay Area		
|MAX|	4.29	0.99	1.12	76.94
MEAN	4.00	0.73	0.96	−74.61
RMSD	4.01	0.77	0.96	74.63

[a]We distinguish between the bay area and the non bay area.

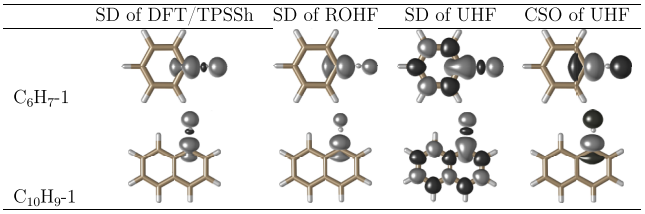
Table 7. Statistics for the Deviations in Activation Energies (in kJ/mol) for the xTB Methods Compared to the TPSSh-D3/TZVP Reference

	GFN1-xTB	GFN2-xTB
	Electronic Contribution	
MAX	35.09	46.43
MEAN	−29.61	−17.34
RMSD	29.70	18.23
	ZPVE Contribution	
MAX	8.13	13.12
MEAN	4.36	−4.37
RMSD	4.42	5.38

Coupled-Cluster Energy Corrections. For correlated wavefunction calculations, apart from the method, two important questions are the basis set convergence and, for radicals, the treatment of the spin. Single-reference coupled-cluster calculations can for radicals be based on unrestricted (UHF) or restricted open-shell (ROHF) Hartree−Fock reference determinants. As mentioned above, it was found at the DFT level that at the transition state and in the product, the spin density of the radical is localized close to the reaction site, essentially in a singly occupied σ-orbital. For the H-abstracted PAH radicals and the transitions states, we observe for unrestricted Hartree−Fock a strong spin-polarization of the orbitals, which also affects the π-system and leads to a delocalization of the spin-density over a large part of the PAH (see Table 8).

We performed UHF-based calculations at the UHF-CCSD(F12*)(T)/aug-cc-pVTZ level for benzene and naphthalene and with PNO-UHF-CCSD(F12*)(T)/aug-cc-pVTZ for phenanthrene. The results are listed in Table 9. In contrast to what one would expect based on the results from DFT, the UHF-coupled-cluster singles-and-doubles with perturbative triples [CCSD(T)] calculations predict that the activation and reaction

Table 8. Spin Densities (SD) of the Transition State Structures for Example Reaction Sites Calculated with DFT/TPSSh-D3, ROHF, and UHF[a]



[a]The last column shows the corresponding spin orbital (CSO) of the UHF wavefunction with occupation closest to 1.

Table 9. UHF-CCSD(F12*)(T)/aug-cc-pVTZ Reaction Energies

	$E_{el,act}$	$E_{el,rxn}$	$(T)_{act}$	$(T)_{rxn}$
C_6H_6	81.7	51.8	−1.9	3.1
$C_{10}H_8$-1	96.4	67.8	1.2	6.7
$C_{10}H_8$-2	90.3	67.0	−3.6	6.5
$C_{14}H_{10}$p-1	109.9	80.5	3.3	8.2
$C_{14}H_{10}$p-5	110.3	75.0	3.1	8.7
$C_{14}H_{10}$a-1	116.6	87.7	9.4	14.4
$C_{14}H_{10}$a-2	117.1	87.3	9.4	14.0
$C_{14}H_{10}$a-3	116.7	86.5	9.3	13.9

energies would increase with the size of the aromatic ring system, for the reaction energy, by ≈16−17 kJ/mol from C_6H_6 to $C_{10}H_8$ and ≈14−23 kJ/mol from $C_{10}H_8$ to $C_{14}H_{10}$. In particular, the perturbative (T) triples correction is for the UHF-based calculations sizeable and grows with the system size.

The counter-intuitive behaviour, however, is an artifact of the spin-polarization and the unphysical delocalization of the spin density over the aromatic ring systems in the UHF reference. With ROHF reference determinants, the spin density is qualitatively similar to that obtained with DFT/TPSSh, as shown in Table 8. The ROHF-CCSD(F12*)(T) results for reaction energies of benzene and naphthalene are shown in Table 10.

Similar as at the DFT level and in agreement with results from Carissan and Klopper[20] at the G3(MP2)-RAD level, which also employs ROHF-CCSD(T) as part of the computational protocol, these results do not increase with the size of the aromatic ring system. Also, the (T) triples correction, which is the most severe computational bottleneck in the coupled-cluster calculations, varies very little between benzene and the two reaction sites at naphthalene. Explicitly correlated CCSD(F12*)/aug-cc-pVTZ results are usually close to the basis set limit, comparable to conventional CCSD/cc-pV5Z results.[27,43] For the reaction energies of H-abstraction from PAHs, both the basis set limits extrapolated from cc-pVDZ and cc-pVTZ result[44]

https://dx.doi.org/10.1021/acs.jpca.0c07133
J. Phys. Chem. A 2020, 124, 9626−9637

Table 10. ROHF-CCSD(T) Reaction Energies and the Contribution of the Triples Correction, (T), to Them in kJ/mol[a]

method	site	$E_{el,act}$	$E_{el,rxn}$	E_{act}	E_{rxn}	$(T)_{act}$	$(T)_{rxn}$
CCSD(T)/cc-pVDZ	C_6H_6	76.5	46.9	69.5	39.0	−3.3	0.7
	$C_{10}H_8$-1	76.8	48.1	70.2	40.7	−3.7	0.7
	$C_{10}H_8$-2	76.6	47.6	69.9	39.6	−3.4	0.7
CCSD(T)/cc-pVTZ	C_6H_6	72.4	41.5	65.4	33.6	−3.6	1.5
	$C_{10}H_8$-1	72.5	42.8	65.9	35.4	−4.0	1.6
	$C_{10}H_8$-2	72.4	42.1	65.7	34.2	−3.7	1.5
extrapolated[b]	C_6H_6	70.9	41.3	63.9	33.5	−3.7	1.9
	$C_{10}H_8$-1	71.1	42.8	64.5	35.4	−4.1	1.9
	$C_{10}H_8$-2	70.9	42.0	64.2	34.1	−3.8	1.9
CCSD(F12*)(T)/aug-cc-pVTZ	C_6H_6	71.8	42.1	64.8	34.3	−3.7	1.6
	$C_{10}H_8$-1	71.9	43.6	65.3	36.2	−4.1	1.6
	$C_{10}H_8$-2	71.8	42.7	65.1	34.8	−3.8	1.6

[a] $E_{act} = E_{el,act} + E_{act,ZPVE}$, $E_{rxn} = E_{el,rxn} + E_{rxn,ZPVE}$. [b] Extrapolated from the cc-pVDZ and cc-pVTZ basis sets.

and the raw cc-pVTZ numbers are close to the CCSD(F12*)-(T)/aug-cc-pVTZ values. For the larger PAHs, we thus continued with PNO-CCSD/cc-pVTZ and added to them the average result for the triples correction from the CCSD(F12*)-(T)/aug-cc-pVTZ calculations, 1.6 kJ/mol for reaction and −3.9 kJ/mol for the activation energies, and the vibrational correction from DFT/TPSSh/TZVP. The results are listed in Table 11. For the benchmark cases, benzene and naphthalene, the results agree within 1 kJ/mol with the CCSD(F12*)(T)/aug-cc-pVTZ reference values.

For the benzene, naphthalene, and phenanthrene accurate results are available in the literature (cmp. Table 12), including an experimental result for the activation energy for benzene.[45] They agree with the results from the current work within ±5 kJ/mol for the reaction and with ±3 kJ/mol for the activation energies, with the exception of the G2M(rcc,MP2) results from ref 46, which are somewhat higher.

Compared to the accurate coupled-cluster results, the DFT/TPSSh/TZVP results significantly underestimate the reaction energies and the activation energies. Closer inspection reveals that for the DFT/TPSSh/TZVP, results differ mainly by a constant offset, for the reaction energies of −20.5 kJ/mol and for the activation energies of −41.1 kJ/mol based on the average over the differences to those given in Table 11.

Extrapolation to Larger PAHs. The analysis of the DFT results showed that most of the site-specific differences between the reaction energies originate from the C−H bond breaking energy. Furthermore, if we distinguish between hindered bay and unhindered sites, the activation energies exhibit an approximately linear relation with the reaction energies (Bell−Evans−Polanyi principle). This allows us to go one step further than above and estimate the reaction and activation energies directly from the C−H bond breaking energies as

$$E_{rxn} = E_{C-H} + E_{relax} + E_{rxn,ZPVE} + E_{rxn,CCSD\text{-}corr} + E_{rxn,(T)}$$

$$E_{act} = E_{BEP} + f_{BEP}(E_{C-H} + E_{relax} + E_{rxn,ZPVE}) + E_{act,CCSD\text{-}corr} + E_{act,(T)}$$

with $E_{relax} = -7.1 \pm 0.4$ kJ/mol, $E_{rxn,ZPVE} = -6.9 \pm 0.8$ kJ/mol, $E_{rxn,CCSD\text{-}corr} = 20.5 \pm 0.3$ kJ/mol, $E_{rxn,(T)} = 1.6$ kJ/mol for the reaction and $E_{act,CCSD\text{-}corr} = 41.1 \pm 0.2$ kJ/mol and $E_{act,(T)} = -3.9$ kJ/mol for the activation energies. $E_{BEP} = 20.397$ kJ/mol and $f_{BEP} = 0.602$ for unhindered and $E_{BEP} = 9.766$ kJ/mol and $f_{BEP} = 2.877$ for bay region sites.

Table 11. PNO-CCSD/cc-pVTZ Results for Hydrogen Abstraction Energies in kJ/mol[a]

site	$E_{el,rxn,CCSD}$	E_{rxn}	$E_{el,act,CCSD}$	E_{act}
C_6H_6	39.9	33.7	75.8	64.9
$C_{10}H_8$-1	41.2	35.5	76.3	65.8
$C_{10}H_8$-2	40.5	34.2	75.9	65.3
$C_{14}H_{10}$a-1	42.8	37.7	77.1	66.8
$C_{14}H_{10}$a-2	41.1	35.2	76.1	65.4
$C_{14}H_{10}$a-3	40.4	33.9	75.9	64.9
$C_{14}H_{10}$p-1	41.2	35.0	76.2	65.4
$C_{14}H_{10}$p-2	41.1	35.3	76.3	65.7
$C_{14}H_{10}$p-3	41.6	35.1	76.7	65.8
$C_{14}H_{10}$p-4	40.5	34.3	75.8	64.8
$C_{14}H_{10}$p-5	34.8	29.3	76.7	67.2
$C_{16}H_{10}$-1	40.7	33.8	75.9	64.9
$C_{16}H_{10}$-2	42.4	36.5	76.9	66.1
$C_{16}H_{10}$-3	40.9	34.6	76.0	65.0
$C_{20}H_{12}$-1	34.0	28.3	77.0	66.6
$C_{20}H_{12}$-2	40.8	36.0	76.0	65.8
$C_{20}H_{12}$-3	42.9	38.6	77.2	67.2
$C_{22}H_{12}$a-1	42.5	37.1	76.9	65.8
$C_{22}H_{12}$a-2	40.6	34.8	75.8	64.9
$C_{22}H_{12}$a-3	42.5	36.6	76.8	65.8
$C_{22}H_{12}$a-4	43.5	40.2	77.4	68.7
$C_{22}H_{12}$a-5	40.8	36.0	75.7	65.7
$C_{22}H_{12}$b-1	35.4	29.3	77.2	68.1
$C_{22}H_{12}$b-2	40.6	35.2	75.8	65.3
$C_{22}H_{12}$b-3	43.0	38.2	77.3	67.0
$C_{22}H_{12}$b-4	41.6	36.8	76.4	66.4
$C_{22}H_{12}$b-5	41.5	36.7	76.4	66.4
$C_{22}H_{12}$b-6	42.1	37.4	76.7	66.7
$C_{24}H_{12}$	41.9	36.9	76.5	66.4

[a] $E_{rxn} = E_{el,rxn,CCSD} + E_{el,rxn,(T)} + E_{rxn,ZPVE}$ with $E_{el,rxn,(T)} = 1.6$ kJ/mol. E_{act} has been calculated correspondingly with $E_{el,act,(T)} = -3.9$ kJ/mol.

For applications in reduced kinetic models that require pretabulated data, calculations for a specific PAH can be replaced by using average values for the reaction site type such as solo sites on zigzag or bay sites on armchair edges. In Table 14, we collected the energy ranges for the seven different site types considered in the current study. With the exception of the K-region duo sites (also known as free edge sites), where the range of the reaction energies 4.3 kJ/mol, the ranges are for all other sites smaller than 1 kcal/mol. This means that the errors

https://dx.doi.org/10.1021/acs.jpca.0c07133
J. Phys. Chem. A 2020, 124, 9626−9637

Table 12. Hydrogen Abstraction Energies by H Atoms from the Literature in kJ/mol

site	method	E_{act}	E_{rxn}
C_6H_6	CCSD(T)-F12a/cc-pVTZ	66.1[47]	33.4[47]
	G2M(rcc,MP2)	83.3[46]	46.4[46]
	CCSD(T)-F12/aug-cc-pVTZ	66.5[48]	35.6[48]
	G3(MP2,CC)	71.1[48]	36.8[48]
	experimental	66.9[45]	36 ± 3[46]
$C_{10}H_8$-1	G3(MP2)-RAD	70[20]	38[20]
	CCSD(T)-F12a/cc-pVTZ	66.5[47]	35.6[47]
$C_{10}H_8$-2	G3(MP2)-RAD	70[20]	37[20]
$C_{14}H_{10}$p-1	G3(MP2)-RAD	70[20]	38[20]
$C_{14}H_{10}$p-2	G3(MP2)-RAD	70[20]	38[20]
$C_{14}H_{10}$p-3	G3(MP2)-RAD	70[20]	38[20]
$C_{14}H_{10}$p-4	G3(MP2)-RAD	63[20]	37[20]
$C_{14}H_{10}$p-5	G3(MP2)-RAD	70[20]	32[20]

[a]Experimental study in a shock tube with laser-schlieren technique over 1900−2400 K and 0.2−1.0 atm.

introduced by taking the average value for the site type are within the error bars of the quantum chemical calculations.

Reaction Rate Constants. The reaction rate constants are calculated using equation 3 based on the energies given in Tables 11 and 13. Table 15 lists the parameters fit to the modified Arrhenius equation for the average over different site types, as classified in Table 14. All reported rate constants are "per reaction site", that is, we excluded the symmetry numbers that account for the summation over symmetry equivalent reaction sites, for example, in benzene or naphthalene, to allow for direct comparability between the different PAHs. The individual rate constants can be found in Supporting Information. As already observed for the activation energies, the armchair bay region sites show the largest variations between the different cases in the test set; therefore, the uncertainty in the rate constant parameters given for the armchair bay region site is higher than the others.

Table 13. Reaction and Activation Energies for Larger Molecules Estimated as $E_{est} = E_{el,DFT} + E_{ZPVE} + E_{CCSD\text{-}corr} + E_{(T)}$ with $E_{rxn,CCSD\text{-}corr}$ = 20.5 kJ/mol, $E_{rxn,(T)}$ = 1.6 kJ/mol, $E_{act,CCSD\text{-}corr}$ = 41.1 kJ/mol, and $E_{act,(T)}$ = −3.9 kJ/mol

site	$E_{rxn,est}$	$E_{act,est}$
$C_{42}H_{18}$-1	30.0	68.7
$C_{42}H_{18}$-2	36.1	65.6
$C_{50}H_{18}$-1	35.3	65.3
$C_{50}H_{18}$-2	29.8	69.1
$C_{50}H_{18}$-3	28.3	63.4
$C_{50}H_{18}$-4	37.0	66.4
$C_{50}H_{18}$-5	36.7	66.4
$C_{50}H_{18}$-6	39.3	67.8
$C_{84}H_{24}$-1	30.2	71.3
$C_{84}H_{24}$-2	38.9	68.8
$C_{96}H_{24}$-1	36.2	66.5
$C_{96}H_{24}$-2	39.5	68.4

Figure 5a shows the average rate constants given in Table 15. In general, the rate constants do not vary significantly with the different sizes and sites of the molecules. The average activation energies (given in Table 14) are ordered as zigzag edge solo sites and armchair bay region sites ≫ K-region duo, inner trio > outer trio, and quartet sites. As can be seen in Figure 5a, the reaction rate constants follow a comparable trend. The armchair bay region and zigzag edge solo sites have the lowest reaction rate constants (56−61 and 41−58% lower compared to free edge outer quartet site respectively). Similarly, the K-region duo sites have around 24−33% lower rate constants compared with the free edge outer quartet sites. Figure 5b shows the calculated rate constants for benzene and naphthalene and compares them with the literature. The calculated reaction rate constant for benzene agree well with the experimental study[45] at the low temperature range. In general, earlier calculations with composite methods, for example, by Semenikhin *et al.*,[48] Kislov *et al.*,[49] and Mebel *et al.*,[46] predict lower rate constants than the ones calculated in this study. The rate constants of the armchair bay region sites are lower than that of the zigzag solo sites (by 9−25%), which is in accordance with the findings of the study by Semenikhin et al. based on G3(MP2,CC) calculations for chrysene and benzo[*a*]pyrene.[48]

SUMMARY AND CONCLUSIONS

Hydrogen abstraction from large polyaromatic systems, as present in (bio)chars or soot, is a crucial first reaction step in heterogeneous combustion mechanism, and the determination of accurate rate parameters is pivotal for its modeling. Because of the systems size, often a single approximate method (e.g., ReaxFF) is used. We showed, however, that multilevel and multimethod approaches are needed to tackle this difficult problem accurately. With a combination of DFT, PNO-CCSD as a local correlation method and CCSD(F12*)(T) as highly accurate method, we extended in the current work the available data on reaction and activation energies and reaction rates from medium-sized systems to large PAHs up to $C_{96}H_{24}$. This has been possible since we could show for small and medium-sized PAHs that the energy corrections for connected triples excitations (T) and also the difference between PNO-CCSD

Table 14. Range of the Reaction Energies (in kJ/mol Including the ZPVE) for Different Types of Reaction Sites, Based on the Results Reported in Tables 11 and 13

site type	sites	E_{rxn}	E_{act}	$E_{act,average}$
zigzag edge solo	$C_{14}H_{10}$a-1, $C_{22}H_{12}$a-4, $C_{50}H_{18}$-6, $C_{96}H_{24}$-2	37.7−40.2	66.8−68.7	67.9 ± 0.8
K-region duo	$C_{14}H_{10}$p-1, $C_{16}H_{10}$-3, $C_{22}H_{12}$a-5, $C_{22}H_{12}$b-4, $C_{22}H_{12}$b-5, $C_{22}H_{12}$b-6, $C_{24}H_{12}$-1, $C_{50}H_{18}$-4, $C_{50}H_{18}$-5, $C_{84}H_{24}$-2, $C_{96}H_{24}$-1	34.7−38.9	65.0−68.8	66.4 ± 1.0
inner trio	C16H12-2, $C_{20}H_{12}$-3, $C_{22}H_{12}$a-1, $C_{22}H_{12}$a-3, $C_{22}H_{12}$b-3	36.6−38.6	65.8−67.2	66.4 ± 0.7
outer trio	$C_{16}H_{10}$-1, $C_{20}H_{12}$-2, $C_{22}H_{12}$a-2, $C_{22}H_{12}$b-2, $C_{42}H_{18}$-2, $C_{50}H_{18}$-1	33.8−36.1	64.9−65.8	65.3 ± 0.3
free edge inner quartet	$C_{10}H_8$-1, $C_{14}H_{10}$a-2, $C_{14}H_{10}$p-2	35.2−35.5	65.4−65.8	65.6 ± 0.2
free edge outer quartet	C_6H_6-1, $C_{10}H_8$-2, $C_{14}H_{10}$a-3, $C_{14}H_{10}$p-3, $C_{14}H_{10}$p-4	33.7−35.1	64.8−65.8	65.1 ± 0.4
armchair bay region	$C_{14}H_{10}$p-5, $C_{20}H_{12}$-1, $C_{22}H_{12}$b-1, $C_{42}H_{18}$-1, $C_{50}H_{18}$-2, $C_{50}H_{18}$-3, $C_{84}H_{24}$-1	28.3−30.2	63.4−71.3	67.8 ± 2.4

https://dx.doi.org/10.1021/acs.jpca.0c07133
J. Phys. Chem. A 2020, 124, 9626−9637

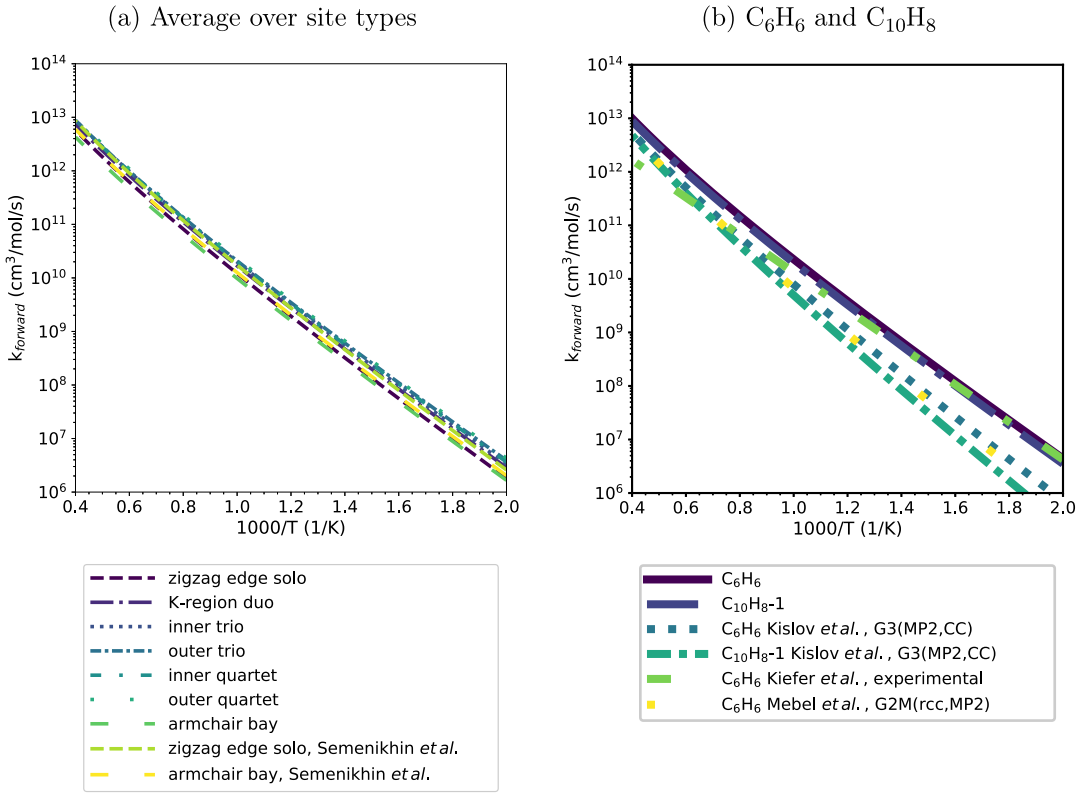


Figure 5. Semi-logarithmic plots of the site specific forward reaction rate constants as a function of inverse temperature for the temperature range 500−2500 K and comparison with the literature. Note that the experimental data for Kiefer *et al.*[45] is based on measurements at a temperature range 1800−2500 K; however, it is shown for the full temperature range. For comparison, the reference rate constants[45,46,49] are divided by 6 for benzene and by 4 for naphthalene so that the per site rate constants can directly be compared.

Table 15. Non-Linear Least Square Fit of the Calculated Rates Constants (k) for the Studied Sites to a Modified Arrhenius Equation, $k = AT^n \exp(-E/T)$, Where T and E Are in Units of K and k is in $cm^3\ mol^{-1}\ s^{-1}$

site type	A	N	E
zigzag edge solo	1.25×10^8	1.76	7585
K-region duo	1.30×10^8	1.78	7437
inner trio	1.82×10^8	1.76	7469
outer trio	1.27×10^8	1.80	7333
free edge inner quartet	1.17×10^8	1.81	7361
free edge outer quartet	1.20×10^8	1.82	7319
armchair bay region	9.62×10^7	1.75	7468

and DFT/TPSSh are transferable between different PAHs and reaction sites. Thus, we can answer the central question, raised in the title, whether small polyaromatics can be used to describe their larger counterparts for local reactions clearly with "yes". In other words, it is at the electronic structure level much more import to use sufficiently accurate methods for smaller models than to approximate the complete system. The effects of steric repulsion and geometric strain, which require at least somewhat larger models, can be described on lower levels with more approximate methods.

In this spirit, it is worth to note that most of the differences in the reaction energies between different sites enter actually via the C−H bond breaking energy at a fixed geometry for the PAH, the computationally cheapest contribution at the DFT level. The activation energies, on the other hand, can for this reaction estimated reliably from the reaction energy, as shown above at the DFT level.

Besides pushing the limits for accurate reference data, we assessed the extended semi-empirical tight binding methods (xTB) and a popular reactive force-field ReaxFF as tools for modeling combustion reactions. The cheapest xTB methods GFN0-xTB are not suitable for modeling combustion since it fails to qualitatively describe H-abstraction by a large order of magnitude. However, GFN2-xTB shows a good agreement with the DFT results in terms of reaction energies and equilibrium geometries, indicating that it could be used in future to bridge between DFT and ReaxFF. Since the latter is numerically the most efficient method, it is ideally suited for an exploration of unknown potential surfaces; however, it strongly overestimates reaction energies and barriers in the studied context, which makes these processes less often observed in an MD simulation, leading to longer simulation times.

Overall we demonstrate that a combination of judiciously chosen methods and exploiting transferability of energetic contributions in a multiscale and multimethod fashion is the ultimate choice for modeling such complex heterogeneous combustion processes, whereas single method strategies will most likely fail.

This work intends to give another contribution toward a better fundamental understanding of the gas/solid heterogeneous reactions. The further confirmation of the possibility of accurately estimating rate constants based on analogous reactions in the gas phase will allow the development of detailed mechanisms to increase the predictability of the actual macromolecular or lumped models.

For the specific reaction class studied in this investigation, the H-abstraction from PAHs with H atoms, we find that the rate

https://dx.doi.org/10.1021/acs.jpca.0c07133
J. Phys. Chem. A 2020, 124, 9626−9637

constants for the sterically unhindered sites can be very well approximated by site type-specific averages.[50] Only for the sterically hindered bay region sites, as found on armchair edges, we observe a significant variation of the rate constants between the cases within the test set. The steric repulsions at these sites induce some non-planarity and geometric strains,[42] partially released when the C−H bond is broken, that depend on the flexibility of the environment.

■ ASSOCIATED CONTENT

Supporting Information

The Supporting Information is available free of charge at https://pubs.acs.org/doi/10.1021/acs.jpca.0c07133.

Study on PNO selection thresholds, non-linear least square fits for the calculated rate constants for the studied sites using a modified Arrhenius equation, additional data for the relation between reaction and activation energy for TPSSh-D3/TZVP, and raw data from our TPSSh-D3/TZVP, xTB and ReaxFF calculations (PDF)

■ AUTHOR INFORMATION

Corresponding Authors

Özlem Yönder − *Lehrstuhl für Theoretische Chemie, Ruhr-Universität Bochum, D-44780 Bochum, Germany;* orcid.org/0000-0002-1464-2018; Email: oezlem.yoender@ruhr-uni-bochum.de

Gunnar Schmitz − *Computational Materials Chemistry Group, Ruhr-Universität Bochum, 44780 Bochum, Germany;* Email: Gunnar.Schmitz@rub.de

Authors

Christof Hättig − *Lehrstuhl für Theoretische Chemie, Ruhr-Universität Bochum, D-44780 Bochum, Germany;* orcid.org/0000-0002-5752-2710

Rochus Schmid − *Computational Materials Chemistry Group, Ruhr-Universität Bochum, 44780 Bochum, Germany;* orcid.org/0000-0002-1933-3644

Paulo Debiagi − *Simulation of Reactive Thermo-Fluid Systems (STFS), TU Darmstadt, 64827 Darmstadt, Germany*

Christian Hasse − *Simulation of Reactive Thermo-Fluid Systems (STFS), TU Darmstadt, 64827 Darmstadt, Germany*

Andrea Locaspi − *Department of Chemistry, Materials and Chemical Engineering "G. Natta", Politecnico di Milano, 20133 Milano, Italy*

Tiziano Faravelli − *Department of Chemistry, Materials and Chemical Engineering "G. Natta", Politecnico di Milano, 20133 Milano, Italy*

Complete contact information is available at: https://pubs.acs.org/10.1021/acs.jpca.0c07133

Notes

The authors declare no competing financial interest.

■ ACKNOWLEDGMENTS

The authors thank the German Research Foundation (DFG) for funding this research within the framework of the SFB/Transregio 129 "Oxyflame" (project number 215035359).

■ ABBREVIATIONS

DFT, density functional theory; CCSD(T), Coupled-cluster singles-and-doubles with perturbative triples; ReaxFF, reactive force field; xTB, extended semi-empirical tight-binding

■ REFERENCES

(1) Paris, O.; Zollfrank, C.; Zickler, G. A. Decomposition and carbonisation of wood biopolymers—a microstructural study of softwood pyrolysis. *Carbon* **2005**, *43*, 53−66.

(2) Amonette, J. E.; Joseph, S. *Biochar for Environmental Management: Science and Technology*; Earthscan, 2009; Chapter 3, pp 34−52.

(3) Keiluweit, M.; Nico, P. S.; Johnson, M. G.; Kleber, M. Dynamic Molecular Structure of Plant Biomass-Derived Black Carbon (Biochar). *Environ. Sci. Technol.* **2010**, *44*, 1247−1253.

(4) Cao, X.; Pignatello, J. J.; Li, Y.; Lattao, C.; Chappell, M. A.; Chen, N.; Miller, L. F.; Mao, J. Characterization of Wood Chars Produced at Different Temperatures Using Advanced Solid-State 13C NMR Spectroscopic Techniques. *Energy Fuels* **2012**, *26*, 5983−5991.

(5) Simmie, J. M. Detailed chemical kinetic models for the combustion of hydrocarbon fuels. *Prog. Energy Combust. Sci.* **2003**, *29*, 599−634.

(6) Kmiecik, S.; Gront, D.; Kolinski, M.; Wieteska, L.; Dawid, A. E.; Kolinski, A. Coarse-Grained Protein Models and Their Applications. *Chem. Rev.* **2016**, *116*, 7898−7936.

(7) van Duin, A. C. T.; Dasgupta, S.; Lorant, F.; Goddard, W. A. ReaxFF: A Reactive Force Field for Hydrocarbons. *J. Phys. Chem. A* **2001**, *105*, 9396−9409.

(8) Salmon, E.; van Duin, A. C. T.; Lorant, F.; Marquaire, P.-M.; Goddard, W. A. Early maturation processes in coal. Part 2: Reactive dynamics simulations using the ReaxFF reactive force field on Morwell Brown coal structures. *Org. Geochem.* **2009**, *40*, 1195−1209.

(9) Castro-Marcano, F.; Kamat, A. M.; Russo, M. F.; van Duin, A. C. T.; Mathews, J. P. Combustion of an Illinois No. 6 coal char simulated using an atomistic char representation and the ReaxFF reactive force field. *Combust. Flame* **2012**, *159*, 1272−1285.

(10) Zheng, M.; Li, X.; Liu, J.; Wang, Z.; Gong, X.; Guo, L.; Song, W. Pyrolysis of Liulin Coal Simulated by GPU-Based ReaxFF MD with Cheminformatics Analysis. *Energy Fuels* **2013**, *28*, 522−534.

(11) Ding, Z.-B.; Di Marco, E.; Pelucchi, M.; Faravelli, T.; Maestri, M. First-principles assessment of the analogy between gas-phase and gas-solid H-abstraction reactions at graphene edges. *Chem. Eng. J.* **2019**, *377*, 119691. , ISCRE 25 Special Issue: Bridging Science and Technology

(12) Lacroix, R.; Fournet, R.; Ziegler-Devin, I.; Marquaire, P.-M. Kinetic modeling of surface reactions involved in CVI of pyrocarbon obtained by propane pyrolysis. *Carbon* **2010**, *48*, 132−144.

(13) Frenklach, M.; Wang, H. Detailed surface and gas-phase chemical kinetics of diamond deposition. *Phys. Rev. B: Condens. Matter Mater. Phys.* **1991**, *43*, 1520−1545.

(14) Wang, H.; Frenklach, M. Calculations of Rate Coefficients for the Chemically Activated Reactions of Acetylene with Vinylic and Aromatic Radicals. *J. Phys. Chem.* **1994**, *98*, 11465−11489.

(15) Adkins, E. M.; Miller, J. H. Towards a taxonomy of topology for polynuclear aromatic hydrocarbons: linking electronic and molecular structure. *Phys. Chem. Chem. Phys.* **2017**, *19*, 28458−28469.

(16) Bell, R. P.; Hinshelwood, C. N. The theory of reactions involving proton transfers. *Proc. R. Soc. London, Ser. A* **1936**, *154*, 414−429.

(17) Evans, M. G.; Polanyi, M. Inertia and driving force of chemical reactions. *Trans. Faraday Soc.* **1938**, *34*, 11−24.

(18) Bannwarth, C.; Ehlert, S.; Grimme, S. GFN2-xTB—An Accurate and Broadly Parametrized Self-Consistent Tight-Binding Quantum Chemical Method with Multipole Electrostatics and Density-Dependent Dispersion Contributions. *J. Chem. Theory Comput.* **2019**, *15*, 1652−1671.

(19) Pracht, P.; Caldeweyher, E.; Ehlert, S.; Grimme, S. *A Robust Non-Self-Consistent Tight-Binding Quantum Chemistry Method for large Molecules*, 2019 DOI: 10.26434/chemrxiv.8326202.v1.

(20) Carissan, Y.; Klopper, W. Hydrogen abstraction from biphenyl, acenaphthylene, naphthalene and phenanthrene by atomic hydrogen and methyl radical: DFT and G3(MP2)-RAD data. *J. Mol. Struct.: THEOCHEM* **2010**, *940*, 115−118.

(21) Staroverov, V. N.; Scuseria, G. E.; Tao, J.; Perdew, J. P. Comparative assessment of a new nonempirical density functional:

Molecules and hydrogen-bonded complexes. *J. Chem. Phys.* **2003**, *119*, 12129−12137.
(22) Treutler, O.; Ahlrichs, R. Efficient molecular numerical integration schemes. *J. Chem. Phys.* **1995**, *102*, 346−354.
(23) Schäfer, A.; Huber, C.; Ahlrichs, R. Fully optimized contracted Gaussian basis sets of triple zeta valence quality for atoms Li to Kr. *J. Chem. Phys.* **1994**, *100*, 5829−5835.
(24) Grimme, S.; Antony, J.; Ehrlich, S.; Krieg, H. A consistent and accurate ab initio parametrization of density functional dispersion correction (DFT-D) for the 94 elements H-Pu. *J. Chem. Phys.* **2010**, *132*, 154104.
(25) TURBOMOLE V7.4 2019, A Development of University of Karlsruhe and Forschungszentrum Karlsruhe GmbH, 1989−2007, TURBOMOLE GmbH, since 2007; available from https://www.turbomole.org.
(26) Csonka, G. I.; Ruzsinszky, A.; Perdew, J. P. Estimation, Computation, and Experimental Correction of Molecular Zero-Point Vibrational Energies. *J. Phys. Chem. A* **2005**, *109*, 6779−6789.
(27) Hättig, C.; Tew, D. P.; Köhn, A. Communications: Accurate and efficient approximations to explicitly correlated coupled-cluster singles and doubles, CCSD-F12. *J. Chem. Phys.* **2010**, *132*, 231102.
(28) Kendall, R. A.; Dunning, T. H.; Harrison, R. J. Electron-affinities of the 1st-row atoms revisited - systematic basis-sets and wave-functions. *J. Chem. Phys.* **1992**, *96*, 6796−6806.
(29) Yousaf, K. E.; Peterson, K. A. *Chem. Phys. Lett.* **2009**, *476*, 303.
(30) Weigend, F.; Köhn, A.; Hättig, C. Efficient use of the correlation consistent basis sets in resolution of the identity MP2 calculations. *J. Chem. Phys.* **2001**, *116*, 3175−3183.
(31) Häser, M.; Ahlrichs, R. Improvements on the direct SCF method. *J. Comput. Chem.* **1989**, *10*, 104−111.
(32) Schmitz, G.; Helmich, B.; Hättig, C. A scaling PNO-MP2 method using a hybrid OSV-PNO approach with an iterative direct generation of OSVs. *Mol. Phys.* **2013**, *111*, 2463−2476.
(33) Schmitz, G.; Hättig, C.; Tew, D. P. Explicitly correlated PNO-MP2 and PNO-CCSD and their application to the S66 set and large molecular systems. *Phys. Chem. Chem. Phys.* **2014**, *16*, 22167−22178.
(34) Development version of TURBOMOLE V7.5 2020, A Development of University of Karlsruhe and Forschungszentrum Karlsruhe GmbH, 1989−2007, TURBOMOLE GmbH, since 2007; available from https://www.turbomole.org.
(35) Aktulga, H. M.; Fogarty, J. C.; Pandit, S. A.; Grama, A. Y. Parallel Reactive Molecular Dynamics: Numerical Methods and Algorithmic Techniques. *Parallel Comput.* **2012**, *38*, 245−259.
(36) Plimpton, S. Fast Parallel Algorithms for Short-Range Molecular Dynamics. *J. Comput. Phys.* **1995**, *117*, 1−19.
(37) Chenoweth, K.; van Duin, A. C. T.; Goddard, W. A. ReaxFF Reactive Force Field for Molecular Dynamics Simulations of Hydrocarbon Oxidation. *J. Phys. Chem. A* **2008**, *112*, 1040−1053.
(38) Extended semi-empirical tight binding model xTB v6.3.1, available from https://github.com/grimme-lab/xtb 2020.
(39) Plessow, P. Reaction Path Optimization without NEB Springs or Interpolation Algorithms. *J. Chem. Theory Comput.* **2013**, *9*, 1305−1310.
(40) Grimme, S. Supramolecular Binding Thermodynamics by Dispersion-Corrected Density Functional Theory. *Chem.—Eur. J.* **2012**, *18*, 9955−9964.
(41) Shavitt, I. A Calculation of the Rates of the Ortho-Para Conversions and Isotope Exchanges in Hydrogen. *J. Chem. Phys.* **1959**, *31*, 1359−1367.
(42) Hemelsoet, K.; Van Speybroeck, V.; Moran, D.; Marin, G. B.; Radom, L.; Waroquier, M. Thermochemistry and Kinetics of Hydrogen Abstraction by Methyl Radical from Polycyclic Aromatic Hydrocarbons. *J. Phys. Chem. A* **2006**, *110*, 13624−13631.
(43) Tew, D. P.; Klopper, W.; Neiss, C.; Hättig, C. Quintuple-ζ quality coupled-cluster correlation energies with triple-ζ basis sets. *Phys. Chem. Chem. Phys.* **2007**, *9*, 1921−1930.
(44) Halkier, A.; Helgaker, T.; Jørgensen, P.; Klopper, W.; Koch, H.; Olsen, J.; Wilson, A. K. Basis-set convergence in correlated calculations on Ne, N2, and H2O. *Chem. Phys. Lett.* **1998**, *286*, 243−252.
(45) Kiefer, J. H.; Mizerka, L. J.; Patel, M. R.; Wei, H. C. A shock tube investigation of major pathways in the high-temperature pyrolysis of benzene. *J. Phys. Chem.* **1985**, *89*, 2013−2019.
(46) Mebel, A. M.; Lin, M. C.; Yu, T.; Morokuma, K. Theoretical Study of Potential Energy Surface and Thermal Rate Constants for the C6H5 + H2 and C_6H_6 + H Reactions. *J. Phys. Chem. A* **1997**, *101*, 3189−3196.
(47) Hou, D.; You, X. Reaction kinetics of hydrogen abstraction from polycyclic aromatic hydrocarbons by H atoms. *Phys. Chem. Chem. Phys.* **2017**, *19*, 30772−30780.
(48) Semenikhin, A. S.; Savchenkova, A. S.; Chechet, I. V.; Matveev, S. G.; Liu, Z.; Frenklach, M.; Mebel, A. M. Rate constants for H abstraction from benzo(a)pyrene and chrysene: a theoretical study. *Phys. Chem. Chem. Phys.* **2017**, *19*, 25401−25413.
(49) Kislov, V. V.; Islamova, N. I.; Kolker, A. M.; Lin, S. H.; Mebel, A. M. Hydrogen Abstraction Acetylene Addition and Diels-Alder Mechanisms of PAH Formation: A Detailed Study Using First Principles Calculations. *J. Chem. Theory Comput.* **2005**, *1*, 908−924.
(50) Violi, A.; Truong, T. N.; Sarofim, A. F. Kinetics of Hydrogen Abstraction Reactions from Polycyclic Aromatic Hydrocarbons by H Atoms. *J. Phys. Chem. A* **2004**, *108*, 4846−4852.

https://dx.doi.org/10.1021/acs.jpca.0c07133
J. Phys. Chem. A 2020, 124, 9626−9637